Varying-Gain Modeling and Advanced DMPC Control of an AFM System

Ningning Qi, Yongchun Fang, *Senior Member, IEEE*, Xiao Ren, and Yinan Wu

Abstract—For an atomic force microscope (AFM) system equipped with a nano-sensor, an accurate varying-gain dynamic model is obtained when considering the piezo-scanner bending effect, which is then utilized to design an advanced discrete-time model predictive controller (DMPC) achieving accurate tracking performance for any given trajectory. Specifically, considering the features of the piezo-scanner in the AFM system, a segmented swept signal with decreasing amplitudes is adopted as the input exerted on the piezo-scanner, with the collected data utilized to set up a dynamic model based on the Numerical algorithm for Subspace State Space System Identification (N4SID) algorithm, where the varying gain is successfully acquired by a polynomial fitting method to increase model precision. Based on the predicted dynamic behavior of the varying-gain model, an advanced DMPC algorithm is designed to fasten the system response and to enhance the robustness of the closed-loop system. The proposed modeling/control strategy is implemented and then applied to a practical AFM system, with the obtained experimental results clearly demonstrating the superior performance of the designed AFM closed-loop control system.

Index Terms—Atomic Force Microscope (AFM), Discrete-Time Model Predictive Control (DMPC), N4SID Algorithm, Tracking Control.

I. INTRODUCTION

WITH the rapid development of nano-technology, an atomic force microscope (AFM) is becoming a more and more important instrument for micro-scale or nano-scale detecting and manipulating tasks in recent years [1], [2], [3]. Since the emergence of this great invention in 1986 [4], AFM has been widely used in a great deal of fields, such as semiconductor industry, food engineering, medicine invention, and so on [5]. To meet the increasing demands from such fields as life science [6], [7], an AFM is expected to achieve better performance for either imaging or nano-manipulation tasks, including higher resolution, faster scanning speed, and wider practicability [8]. Therefore, more and more attention has been paid on an AFM itself, aiming to provide a more versatile instrument for important research topics, such as genetic engineering [9], through either better hardware components [10], [11], or more advanced algorithms [12].

Currently, a piezo-scanner has been generally selected as the actuator of an AFM system due to its merits of fast response and high resolution. However, the nonlinearities of the piezo-scanners, mainly including hysteresis [13], creep,

drift, vibrational dynamics, and so on, badly limit the scanning speed and imaging precision of an AFM system [14]. Therefore, the control problem for an AFM, mainly addressing the nonlinearities of its piezo-scanner, has recently been put on the agenda within the nano-scale engineering community [15], with emphasis on both horizontal (x/y-axis) and vertical (z-axis) directions. For instance, A charge amplifier exploited by Fleming is utilized to keep the imaging hysteresis within 1% [16], yet the complexity of the circuit design is correspondingly increased as some side effect. An asymmetric Prandtl-Ishlinskii (PI) model is proposed to describe the hysteresis of a piezo-scanner, while an inverse model-based feedforward controller is implemented to achieve precise positioning in [17]. Meanwhile, in [18], an image-based approach is proposed to model and then compensate for the hysteresis behavior of the studied piezo-scanner, and an extended PI model is put forward to address the hysteresis and creep effect for nano-manipulation tasks in [19], with thermal drift compensated by such methods as local scan algorithm [20]. Besides, Zou *et al.* design an inversion-based iterative control technique to shorten the response time of an AFM, by compensating for both the hysteresis and vibrational effects of a piezo-scanner [21]. Later on, a model-free inversion-based iterative feedforward control approach is further proposed, also by Zou *et al.*, to enhance the robustness of the AFM control system [22].

As generally known, an AFM scans a sample through a raster way, and it usually takes several minutes to obtain a high-quality image for the surface of the detected sample. However, to supervise some chemical or biological processes on-line, much higher scanning speed is needed without much compromise on image quality. Based on this observation, some researchers have started to address the problem of generating a reliable image while satisfying the time constraint simultaneously. So far, two mainstream methods have been studied extensively. The first one aims to utilize transient data to construct an accurate image for the sample [23], [24], while more efforts have been put on the latter one of designing various advanced control strategies to fasten the transient process [25], [26]. In [27], an empirical variable-speed scanning (VSS) method is proposed to implement high-speed scanning, which introduces an online auto-tuning mechanism to properly distribute the imaging time along sample surface. To improve transient response, a Lyapunov-based robust adaptive controller is developed and then implemented for a piezo-scanner in [28] by the utilization of a high-precision displacement sensor. In [29], an output feedback robust adaptive control (OFRAC) law is designed to improve the control performance of high-speed tasks, which successfully solves sensor saturation and various disturbance rejection problem. Recently, some compliant XY/XYZ nano-positioners are employed as

actuators for AFMs, whose cross-coupling effect [30] cannot be ignored for high-speed raster scanning, and some control strategies are thus designed in [31] to minimize the X-Y cross-coupling motions. More recently, predictive control strategy, which presents the advantages of short setting time and good control precision, has been introduced for AFM control. For example, in [32], an observer-based model predictive control scheme is presented to achieve accurate tracking control for an AFM system, with a notch filter employed to deal with the resonant mode of a piezo-scanner, and a Kalman state observer constructed to reduce the effect of system measurement noise. Xu *et al.* propose an enhanced model predictive discrete-time sliding mode control (MPDSMC) in [33] to enable an AFM to track a given trajectory without much chattering problem.

It is worthwhile to point out that, though the AFM control problem has recently received considerable attention and many results have been reported so far, the problem is yet far from being solved due to the fact that the currently existing methods often present the following two problems: 1) it usually takes comparatively long time to stabilize the control system around a steep point on the sample surface, which then badly limits the scanning speed of an AFM system; 2) some advanced control algorithms, though theoretically proven to provide superior performance, are unfortunately too complex to be utilized in a practical AFM system. Based on these observations and inspired by the results of [32] and [33], this paper designs a model-predictive control algorithm based on a novel varying-gain model to implement high-speed scanning tasks, whose validity is sufficiently demonstrated via various experimental tests and practical applications. Specifically, a varying-gain model is set up for an AFM system by the utilization of the N4SID algorithm and a polynomial fitting method, based on which, an advanced DMPC control algorithm is then constructed to achieve superior control performance, mainly in terms of fast response speed and good robustness. The designed control strategy is implemented, tested and then employed to scan certain samples, with collected results clearly demonstrating the validity of the AFM control system. Compared with existing work, the contribution of the paper mainly lies in the following three aspects: 1) the construction of an original varying-gain model which describes the characteristics of a scanner-sensor unit with much higher accuracy; 2) development and implementation of a high-performance DMPC-based AFM control system; 3) successful application of the designed AFM control system over practical samples.

The remainder of this paper is organized as follows. Section II briefly introduces the schematic diagram of a typical AFM. System modeling is accomplished in Section III, mainly focusing on dynamic model development and varying gain determination. In Section IV, an advanced DMPC controller is developed based on the obtained varying-gain model, which is then implemented and sufficiently tested in Section V. Finally, Section VI concludes this paper.

II. CLOSED-LOOP SYSTEM DESCRIPTION

As shown in Fig. 1, a typical AFM is composed of the following four parts: a piezo-scanner, a probe/microcantilever,
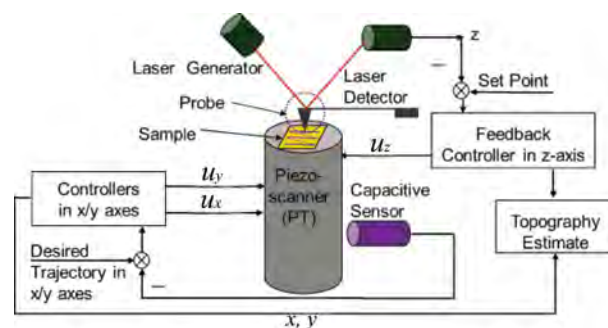

Fig. 1. Schematic diagram of an AFM system.

a laser and a position sensitive photodiode (PSPD) to detect the cantilevers deflection, and controllers in x, y, z three directions. The working principle of an AFM can be described as obtaining surface topography information for a sample which is placed on the piezo-scanner, by the indirect utilization of the interactive force between the probe tip and the sample. Choosing different types of feedback signals in z axis to complete the control loop, either the deflection of its micro-cantilever, or the changes in oscillation amplitude/resonance frequency of its microcantilever, an AFM can be used in contact mode or non-contact mode.

At present, a kind of single-tube piezo-scanner with high resolution is generally used as the actuator of an AFM system, with the x, y directions controlled via the open-loop manner. Unfortunately, the piezoelectric nonlinearities, such as hysteresis, creep, drift, cross-coupling and vibrational dynamics, affect the response speed and control precision of the scanner, which then decreases the scanning or nano-manipulation performance sharply. In this paper, to address the previous problem, a capacitive sensor, as shown in Fig. 1, is installed in the AFM system to detect the displacement of the piezo-scanner in x or y axis, whose measurement is then utilized as the feedback to implement possible closed-loop control. Based on the constructed closed-loop AFM system along the x or y axis, some modeling and control algorithms are then designed to decrease positioning error, with the performance verified by experimental results over practical samples. Considering the symmetry in x and y axes, without loss of generality, the sub-system in x direction is taken as an example in the following parts to demonstrate the modeling and control design strategy.

III. SYSTEM MODELING

A. Dynamic Modeling

To identify the dynamic model of an AFM system, a series of input signal is exerted on the system, whose response is measured and then utilized to determine the model. Generally, white noise or sweep signal of sufficiently large amplitude is often selected as the excitation signal for the system, aiming to collect data completely covering working range and valid frequency scope, so as to identify an accurate model for the system. Unfortunately, such an excitation signal has to take the risk of possibly damaging the piezo-scanner. To avoid

this problem, the following segmented sweep signal with decreasing amplitudes, denoted as $s(t) \in \mathbb{R}$, is designed as the excitation signal for the system:

$$s(t) = \begin{cases} (135 - 26t)\cos(20\pi t^2 + \frac{\pi}{2}), & 0 \leq t \leq 2.5 \\ (110 - 16t)\cos(20\pi t^2 + \frac{\pi}{2}), & 2.5 < t \leq 5 \\ (59 - 5.8t)\cos(20\pi t^2 + \frac{\pi}{2}), & 5 < t \leq 10 \\ \cos(20\pi t^2 + \frac{\pi}{2}), & 10 < t \leq 50 \end{cases} \quad (1)$$

where the frequency range of $s(t)$ is selected from 0 Hz to 1 kHz due to the fact that the first resonant frequency $\omega_r < 1$ kHz for the studied system, with the unit of time t selected as second. From the expression of the signal $s(t)$, it can be seen that the amplitude of $s(t)$ drops rapidly when the frequency is less than 50 Hz as $0 \leq t \leq 2.5$, and the declining rate decreases gradually with the increase of the frequency. Specially, the amplitude is maintained at 1 V when the frequency is larger than 200 Hz as $10 \leq t \leq 50$. The input signal is exerted on the piezo-scanner and the caused displacement is then detected by the equipped capacitive sensor, with the measurement recorded as the output. Therefore, the model not only includes the characteristics of the piezo-scanner, but also the features of the capacitive sensor. The input and output signals of the experiment are shown in Fig. 2, from which it can be seen that the first resonant frequency is approximately 585 Hz.
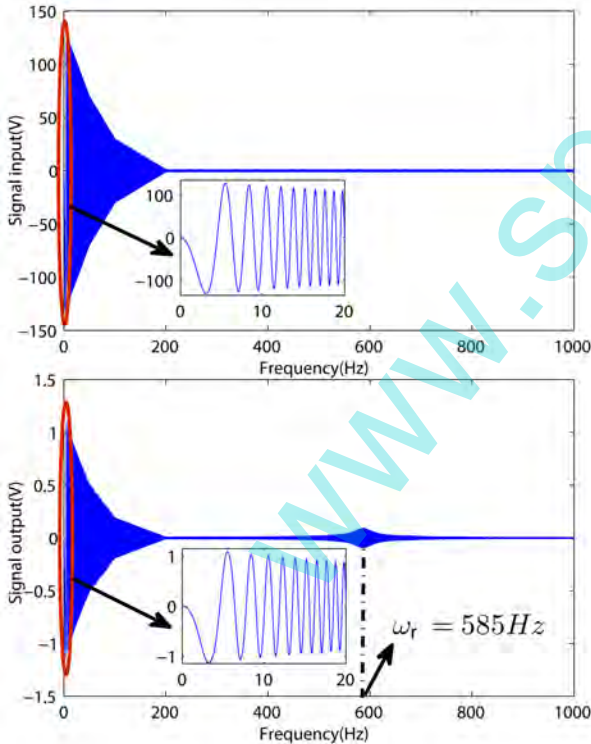

Fig. 2.   Input and output signals of the system.

In order to reduce the sensor noise effect on the acquired data, a low-pass filter is utilized to pre-process the input and output signals, based on which, a discrete-time state-space model is obtained by the N4SID algorithm [34], which is then converted into the following 5th order dynamic discrete-time

transfer function:

$$G(z) = \frac{b_4 z^4 + b_3 z^3 + b_2 z^2 + b_1 z + b_0}{z^5 + a_4 z^4 + a_3 z^3 + a_2 z^2 + a_1 z + a_0}, \quad (2)$$

where the coefficients $a_i, i = 0, 1, ...4, b_j, j = 0, 1, ...4$ are experimentally determined as follows:

$$\begin{bmatrix} a_0 \\ a_1 \\ a_2 \\ a_3 \\ a_4 \end{bmatrix} = \begin{bmatrix} -0.5811 \\ 2.9304 \\ -6.2957 \\ 7.1119 \\ -4.1654 \end{bmatrix}, \begin{bmatrix} b_0 \\ b_1 \\ b_2 \\ b_3 \\ b_4 \end{bmatrix} = \begin{bmatrix} -7.3111 \times 10^{-4} \\ 2.2246 \times 10^{-3} \\ -2.5832 \times 10^{-3} \\ 1.3504 \times 10^{-3} \\ -2.5958 \times 10^{-4} \end{bmatrix}. \quad (3)$$

The Bode plots of model (2) are provided in Fig. 3, together with the real system dynamics, where the red dashed line and blue solid line respectively represent the frequency response of the system dynamics and the identified model $G(z)$. It can be seen that the model matches the system dynamics very well. Besides, the first resonance frequency can be determined from Fig. 3 as $\omega_{rm} = 586.5$ Hz, which is almost identical with that of the real system, denoted as ω_r in Fig. 2. This fact clearly indicates the accuracy of the model. Besides, we will also test the precision of the model via further experiments in the next sub-section.
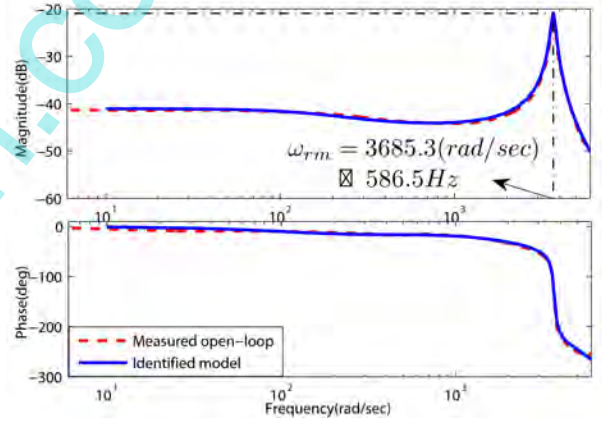

Fig. 3.   Bode plots of the system dynamics and the identified model.

B. Model Evaluation and Improvement

The input and output signals are used to test and verify the accuracy of model (2), with the verification error shown in Fig. 4, from which we can calculate the relative root mean square (RMS) error E_{rms}:

$$E_{rms} = \frac{||y_{real} - y_{model}||_2}{||y_{real}||_2} \times 100\% = 6.99\% \quad (4)$$

where y_{real} and y_{model} are the outputs of the real system and model (2) for the same excitation signal (1), respectively. As indicated by the error data shown in Fig. 4, model (2) describes the dynamic characteristics of the AFM system with satisfactory accuracy.

For an AFM system, a raster scan pattern is the most frequently utilized scanning mode, which uses a triangle waveform in the x-direction and a linear ramp in the y-direction. In [35], a new spiral scan pattern is proposed for fast
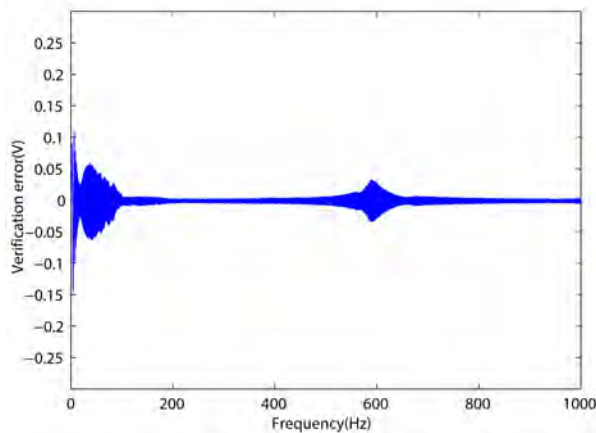
Fig. 4.   Verification error results of $G(z)$.

Fig. 5.   Verification results of model $G(z)$ for triangular waveform of 1 Hz, 10 μm.

AFMs by employing sinusoidal waveforms. Based on these facts, some triangular and sinusoidal waveforms are selected as the desired trajectories and then applied to the AFM system to test the accuracy of model (2). After numerous experiments, it is found that the input-output gain of the system varies for different frequency or amplitude of the input signals. For example, when the scan frequency and range are set as 1 Hz and 10 μm respectively, the experimental results are provided in Fig. 5, where the output of the model is slightly larger than the capacitive sensor measurement regarded as real output.

Based on this observation, we define an adjustment coefficient k to reflect the variation of the input-output gain, which will be subsequently determined via experimental results:

$$k = \frac{V_r}{V_m} \tag{5}$$

where V_r and V_m denote the amplitudes of the outputs for the real system and model (2), respectively. Many experiments have been conducted to determine the adjustment coefficient, and the results collected at 1 Hz and 5 Hz for different triangular waveforms are shown in Table I. As clearly indicated from these results, k is mainly related to the scanning range y, it raises as the increase of the scanning range. As can be also seen from the results of Table I, for fixed scanning range, the coefficient k hardly changes with different scanning frequencies. Therefore, scanning range is regarded as the main factor for the variation of the coefficient k, while the effect of frequency difference is subsequently ignored without sacrificing much precision.

Fig. 6 plots the schematic diagram of the piezo-scanner tube (PT) and the capacitive sensor. After some mathematical analysis, it can be concluded from Fig. 6 that:

$$\frac{\Delta h'}{\Delta h} = \frac{l_1}{l} \frac{1}{\cos(\alpha)} > 0 \tag{6}$$

where Δh, $\Delta h'$ denote the movement of the PT, and the variation for the distance between the piezo-scanner and the capacitive sensor, which are proportional to V_m and V_r respectively. α is the piezo-scanner bending angle. In (6), l_1 stands for the fixed displacement between the normal of the sensor probe surface and the bottom of the piezo-scanner, and l
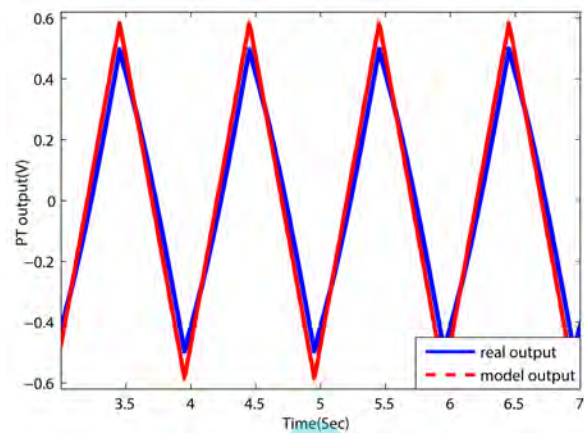
TABLE I
VERIFICATION RESULTS OF MODEL $G(z)$ FOR TRIANGULAR WAVEFORM

Range	1 Hz			5 Hz		
$y(nm)$	$V_r(V)$	$V_m(V)$	$k = V_r/V_m$	$V_r(V)$	$V_m(V)$	$k = V_r/V_m$
8000	0.762	0.939	0.813	0.730	0.903	0.809
9000	0.876	1.056	0.829	0.840	1.016	0.827
10000	0.998	1.173	0.851	0.952	1.129	0.844
11000	1.112	1.291	0.862	1.068	1.242	0.860
12000	1.236	1.408	0.878	1.186	1.354	0.876
13000	1.361	1.525	0.892	1.308	1.467	0.892
14000	1.488	1.642	0.906	1.432	1.580	0.906
15000	1.623	1.760	0.922	1.556	1.693	0.919
16000	1.755	1.877	0.935	1.686	1.806	0.934
17000	1.891	1.995	0.948	1.815	1.919	0.946
18000	2.029	2.112	0.961	1.946	2.032	0.958
19000	2.171	2.229	0.974	2.080	2.145	0.970
20000	2.316	2.347	0.987	2.217	2.257	0.982

is the length of the piezo-scanner, which is assumed invariable when the piezo-scanner bends along the horizontal directions, since the variation of α is relatively small during the scanning process. Based on the previous analysis, (5) can be combined with (6) to obtain:

$$k \propto \frac{1}{\cos(\alpha)}. \tag{7}$$

As shown in Fig. 6, α increases as the scanning range y grows, which then decreases $\cos(\alpha)$ and subsequently increases k, as clearly indicated from (7).

From the previous anaylsis, it is clear that the variation of the coefficient is caused by the angle between the capacitive sensor surface and the piezo-scanner. When installing the capacitive sensor, it is nearly impossible to make the surface of the capacitive sensor completely parallel with the normal plane of the piezo-scanner. Moreover, the parallelism is further reduced when the scanning range of the AFM increases, due to the bending movement of the piezo-scanner, which then leads to the inaccuracy reflected in Table I. Therefore, the dynamic linear model (2) cannot well describe the nonlinearity caused by sensor measurement, and large error occurs when scanning a sample in large range (see Table I). To address this kind of measurement nonlinearity, a polynomial fitting method is
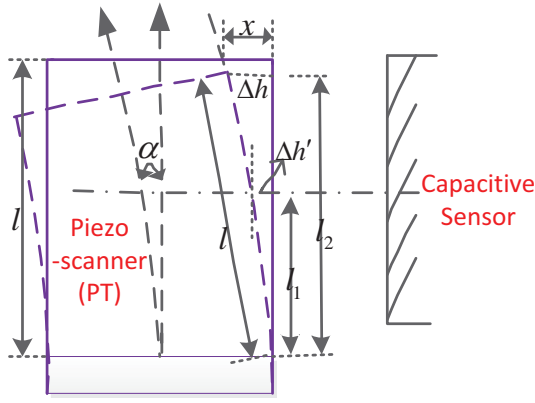
Fig. 6.   Schematic diagram of the piezo-scanner and the capacitive sensor.

employed to calculate the variation of the coefficient k defined in (5), by utilizing the triangular waveform experimental data of $1 \sim 20$ μm at 1 Hz. Afterwards, an improved model is constructed by introducing the varying gain into the original model (2) as follows:

$$G_m(z) = k(y) \times G(z) \tag{8}$$

where $k(y)$ is the varying gain, which, as pointed out previously, is mainly related with the scanning range y. After some tedious analysis for the collected experimental data, the adjustment coefficient $k(y)$ is expressed as a 5th order polynomial:

$$k(y) = -4.39 \times 10^{-22}y^5 + 2.67 \times 10^{-17}y^4 - 6.06 \times 10^{-13}y^3$$
$$+ 6.12 \times 10^{-9}y^2 - 9.30 \times 10^{-6}y + 0.713, \tag{9}$$
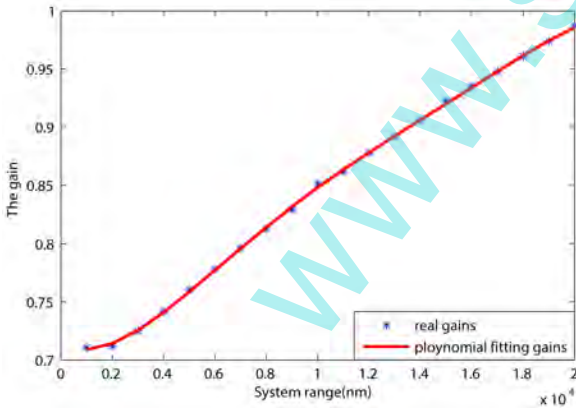
with the fitting results shown in Fig. 7.

Fig. 7.   Fitting results of the coefficient $k(y)$.

To further investigate the performance of the proposed varying-gain model (8), triangular and sinusoidal waveform input/output signals under different frequencies and different ranges are obtained by several additional sets of experiments. Fig. 8 and Fig. 9 plot two sets of those verification results, corresponding to a sinusoidal waveform of 10 Hz, 10 μm, and a triangular waveform of 5 Hz, 20 μm, respectively, where the solid and dashed lines represent the outputs of the real

system and model (8), respectively. From these figures, it can be seen that the improved varying-gain model (8) describes the characteristics of the scanner-sensor unit with sufficiently high precision.

Remark 1: The variation of the gain k is caused by both the proposed bowing effect and the nonlinear characteristics of the piezo-tube. By employing a polynomial fitting method, both factors can be successfully considered in the model.
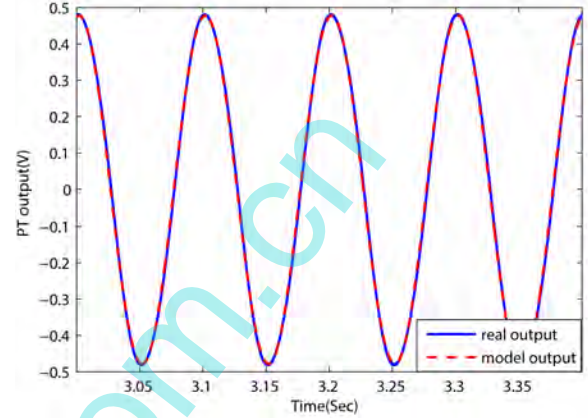

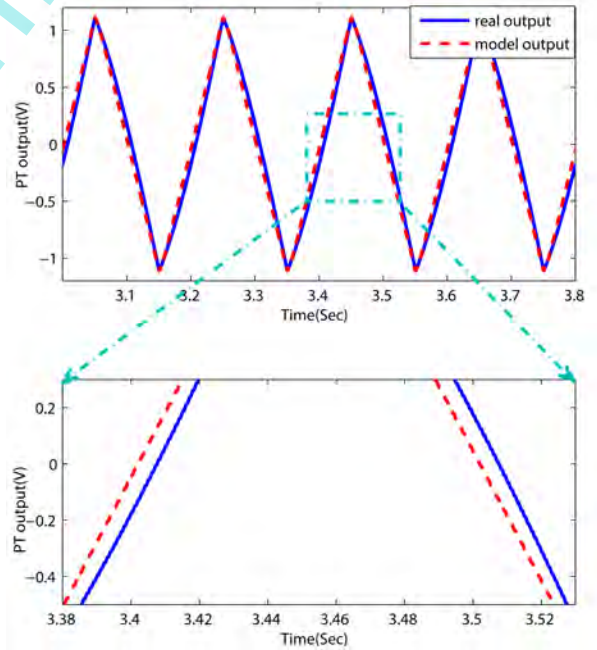Fig. 8.   Verification results of model $G_m(z)$ for a sinusoidal waveform of 10 Hz, 10 μm.

Fig. 9.   Verification results of model $G_m(z)$ for a triangular waveform of 5 Hz, 20 μm.

IV. DMPC CONTROLLER DESIGN

To deal with the time varying and nonlinear behaviors of the studied AFM system, based on the constructed varying-gain dynamic model, an advanced discrete-time model predictive controller is proposed, with the motivation of fully utilizing

the advantages of the DMPC algorithm, including predicted accuracy and optimal performance [36], so as to achieve superior tracking performance for fast AFM scanning tasks.

The structure of the DMPC algorithm designed for the piezo-scanner is shown in Fig. 10, where $y_r(k)$, $u(k)$ and $y(k)$ are the desired trajectory, the control input and the measurement of the capacitive sensor at the k-th sampling period. Specifically, the DMPC algorithm consists of a discrete-time predictive model whose output is denoted as $Y_p(k)$, a trajectory soften element aiming to generate the smooth trajectory $Y_d(k)$, and a rolling optimization component to finally calculate a best control input $u(k)$ for the system.
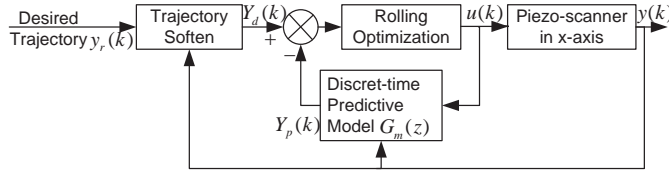

Fig. 10.   Structure of the DMPC algorithm.

To facilitate the controller design, the varying-gain model (8) is rewritten into the following state-space form:

$$x_m(k+1) = A_m x_m(k) + B_m u(k)$$
$$y(k) = C_m x_m(k) \qquad (10)$$

where $u(k) \in \mathbb{R}$ is the control input, $y(k) \in \mathbb{R}$ denotes the output measurement by the capacitive sensor, $x_m \in \mathbb{R}^{5 \times 1}$ denotes the state variable, and the matrices A_m, B_m and C_m are explicitly defined as follows:

$$A_m = k(y) \begin{bmatrix} 0 & 1 & 0 & 0 & 0 \\ 0 & 0 & 1 & 0 & 0 \\ 0 & 0 & 0 & 1 & 0 \\ 0 & 0 & 0 & 0 & 1 \\ -a_0 & -a_1 & -a_2 & -a_3 & -a_4 \end{bmatrix}$$
$$B_m = \begin{bmatrix} 0 & 0 & 0 & 0 & 1 \end{bmatrix}^T$$
$$C_m = \begin{bmatrix} b_0 & b_1 & b_2 & b_3 & b_4 \end{bmatrix}, \qquad (11)$$

with $a_0 \sim a_4$, $b_0 \sim b_4$ and $k(y)$ defined previously.

To decrease the tracking error, the predicted state-space model with embedded integrator can be set up on the increment of the state variable Δx_m, which is explicitly expressed as:

$$\overbrace{\begin{bmatrix} \Delta x_m(k+1) \\ y(k+1) \end{bmatrix}}^{x(k+1)} = \overbrace{\begin{bmatrix} A_m, 0_m^T \\ C_m A_m, 1 \end{bmatrix}}^{A} \overbrace{\begin{bmatrix} \Delta x_m(k) \\ y(k) \end{bmatrix}}^{x(k)} + \overbrace{\begin{bmatrix} B_m \\ C_m B_m \end{bmatrix}}^{B} \Delta u(k)$$
$$y(k) = \overbrace{\begin{bmatrix} 0_m, 1 \end{bmatrix}}^{C} \begin{bmatrix} \Delta x_m(k) \\ y(k) \end{bmatrix}, \qquad (12)$$

where the increments of the variables are defined as

$$\Delta x_m(k+1) = x_m(k+1) - x_m(k) \qquad (13)$$
$$\Delta u(k) = u(k) - u(k-1), \qquad (14)$$

A, B and C are the corresponding augmented matrices, while $x(k)$ denotes the augmented state variable.

Particularly, it is worthwhile to point out that drastic changes of control inputs tend to excite the oscillation of the piezo-scanner, which occurs frequently at the beginning of the tracking process, mainly due to the large initial error. To avoid this problem, a smooth reference trajectory, defined as $Y_d(k)$ previously, is designed as follows:

$$Y_d(k) = [y_d(k+1|k), \cdots, y_d(k+j|k), \cdots, y_d(k+N_p|k)]^T$$
$$y_d(k+j|k) = \beta^j y(k) + (1-\beta^j) y_r(k) \qquad (15)$$

where $y(k)$ and $y_r(k)$ have been previously defined, $y_d(k+j|k)$ denotes the predicted reference trajectory for the subsequent N_p sampling periods at current time k, with N_p being the prediction horizon, and $\beta \in [0,1)$ is called the smooth factor.

To obtain a best control input meeting various conditions, rolling optimization is implemented to ensure that the predicted output $Y_p(k)$ of model (8) is close enough to the smooth reference trajectory $Y_d(k)$, and simultaneously to reduce the vibration of the piezo-scanner caused by possible severe control changes. To this end, the cost function J reflecting the control objective is defined as follows:

$$J = (Y_p(k) - Y_d(k))^T (Y_p(k) - Y_d(k)) + \Delta U(k)^T R \Delta U(k) \qquad (16)$$

where

$$Y_p(k) = [y(k+1|k), \cdots, y(k+j|k), \cdots, y(k+N_p|k)]^T$$
$$\Delta U(k) = [\Delta u(k), \cdots, \Delta u(k+i), \cdots, \Delta u(k+N_c-1)]^T, \qquad (17)$$

$1 \le j \le N_p$, $0 \le i \le N_c - 1$, and N_p, N_c are the prediction horizon and control horizon respectively, with $N_c \le N_p$, and R represents the diagonal, control factor matrix.

In addition, the predicted augmented state variable, together with the output, can be deduced from (12) as:

$$x(k+1|k) = Ax(k) + B\Delta u(k)$$
$$x(k+2|k) = Ax(k+1|k) + B\Delta u(k+1)$$
$$= A^2 x(k) + AB\Delta u(k) + B\Delta u(k+1)$$
$$\vdots$$
$$x(k+N_p|k) = A^{N_p} x(k) + A^{N_p-1} B\Delta u(k) + \cdots$$
$$+ A^{N_p-N_c} B\Delta u(k+N_c-1)$$
$$y(k+j|k) = Cx(k+j|k), 1 \le j \le N_p. \qquad (18)$$

Subsequently, the predicted output $Y_p(k)$ can be calculated by substituting (18) into (17):

$$Y_p(k) = Fx(k) + \Phi \Delta U(k)$$
$$F = \begin{bmatrix} CA & CA^2 & \dots & CA^{N_p} \end{bmatrix}^T$$
$$\Phi = \begin{bmatrix} CB & 0 & \dots & 0 \\ CAB & CB & \dots & 0 \\ \vdots & & & \\ CA^{N_p-1}B & CA^{N_p-2}B & \dots & CA^{N_p-N_c}B \end{bmatrix}. \qquad (19)$$

Substituting (19) into (16) yields:

$$J = [Fx(k) + \Phi \Delta U(k) - Y_d(k)]^T [Fx(k) + \Phi \Delta U(k) - Y_d(k)] + \Delta U(k)^T R \Delta U(k). \qquad (20)$$

To enable J to reach its minimum, its partial derivative needs to satisfy the following constraint:

$$\frac{\partial J}{\partial \Delta U(k)} = 0. \tag{21}$$

Based on this fact, we can take the partial derivative of J regarding $\Delta U(k)$, make some mathematical arrangement for the resulting expression, and then utilize (21) to obtain:

$$(Fx(k) - Y_d(k))\Phi^T + (\Phi^T\Phi + R)\Delta U(k) = 0, \tag{22}$$

which yields the solution of the optimal input $\Delta U(k)$:

$$\Delta U(k) = (\Phi^T\Phi + R)^{-1}\Phi^T Y_d(k) - (\Phi^T\Phi + R)^{-1}\Phi^T Fx(k), \tag{23}$$

where $(\Phi^T\Phi + R)^{-1}\Phi^T Y_d(k)$ corresponds to the change of the reference trajectory, while the term $-(\Phi^T\Phi + R)^{-1}\Phi^T Fx(k)$ stands for the state feedback within the DMPC framework. The first element of the control increment vector $\Delta U(k)$, denoted as $\Delta u(k)$, is selected as the incremental control input, which is finally utilized to calculate the control signal applied to the piezo-scanner as follows:

$$u(k) = u(k-1) + \Delta u(k). \tag{24}$$

Remark 2: By investigating the Bode plots of the system, the stability of the designed DMPC control system is guaranteed. Yet, considering that this is a fairly standard way, it is excluded from the manuscript due to the space limitation.

V. EXPERIMENTS AND APPLICATIONS

To verify the validity of the established varying-gain model and the designed DMPC controller, a closed-loop system is constructed by equipping a capacitive sensor with a Benyuan CSPM 4000 AFM system. The hardware architecture of the experimental platform is shown in Fig. 11, where a single-tube piezo-scanner with range of $20 \times 20 \times 4 \, \mu m$ provided by Benyuan company is selected as the actuator of the system. In Fig. 11, $y_r(k)$ denotes the desired trajectory defined pre-
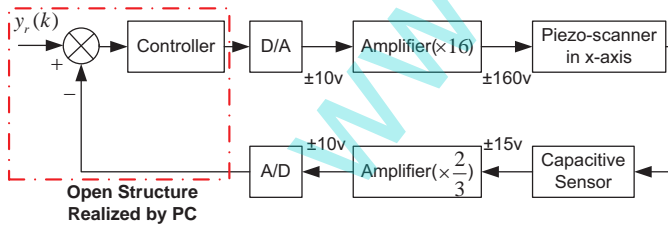

Fig. 11. Hardware architecture of the studied AFM.

viously, which is calculated, together with the modeling and control algorithm, in the RT-Linux platform within a personal computer (PC). Specifically, two input/output channels have been additionally added into the constructed real-time control system, so as to implement feedback tracking control. For the hardware given in Fig. 11, D/A and A/D cards are adopted as PCI-9111HR and PCI-6208V respectively, both of which are produced by Adlink company. The ADE 8810 capacitive sensor, supplied by ADE technologies, is utilized to measure

the displacement of the piezo-scanner with the bandwidth of 10 kHz. Besides, to ensure voltage matching between various modules, two different amplifiers are employed in the system.

A. Tracking Control for Reference Signals

Currently, for an AFM system, a trajectory with triangular or sinusoidal waveform is usually applied to the x-axis in the well-established raster scan pattern. Based on this fact, the proposed DMPC algorithm is employed for the tracking control of triangular/sinusoidal waveforms at different frequencies, while a conventional proportional-integral (PI) controller, which prevails in current available AFMs, is also implemented to enable comparison. To acquire better performance, both the DMPC and PI control laws have been well tuned through sufficient tests, which yields the following gains for the PI controller:

$$k_p = 0.1, k_i = 2000,$$

and

$$\beta = 0.1, N_p = 20, N_c = 2, R = 0.005I_{2\times 2}$$

for the designed DMPC law. These control gains are then kept constant, and are always utilized for the other experiments. That is, we have adopted the following steps to implement several experiments, with the motivation of testing its tracking precision, and its adaptability for different conditions: 1) under a specific scanning frequency, the control gains are sufficiently tuned to yield best performance; 2) the scanning frequency is then increased, while the control gains are kept constant to scan and then image the sample. To enable comparison, the conventional PI controller is tested under the same conditions.

Triangular Waveform Tracking Control: To investigate the performance of both controllers, we first test them by triangular waveforms under different frequencies of 5 Hz, 20 Hz, and 50 Hz. The experimental results are shown in Fig. 12 ∼ Fig. 14, with the top curve plotting the output of the system and the bottom one representing the tracking error, where the black dashed line is the desired trajectory, the red solid and blue dot-dashed lines represent the tracking performance of DMPC controller and PI controller respectively. It is not difficult to see from these figures that the proposed DMPC control yields much better performance than the conventional PI controller, and the feat of the DMPC algorithm becomes more and more apparent with the increase of the scanning frequency. It should be noted that when the scanning frequency is very high, such as 20 Hz and 50 Hz, the tracking performance of DMPC algorithm is not good enough due to the reason that the system cannot reach steady-state for certain steep points, yet it is still possible to obtain acceptable images from these results of DMPC controller, while currently utilized PI control law cannot provide any useful information under this scanning speed.

Sinusoidal Waveform Tracking Control: We fully test the performance of both controllers with sinusoidal waveform under different scan frequencies. Yet, only the results for 20 Hz is provided in Fig. 15, due to space limitation. It can be seen from this figure that compared with the conventional PI
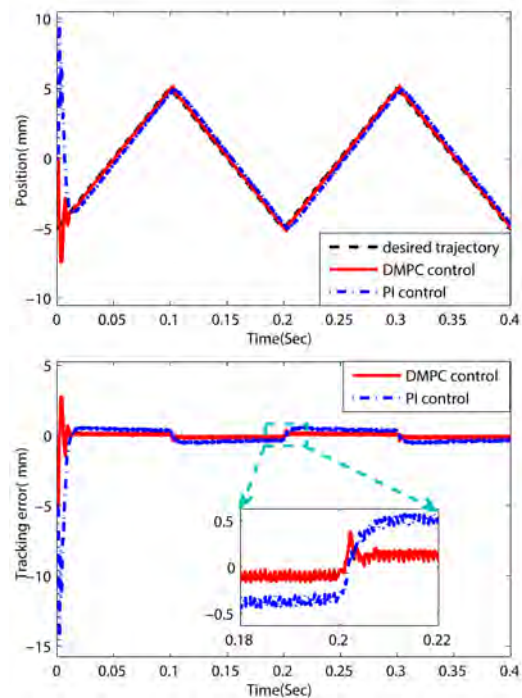
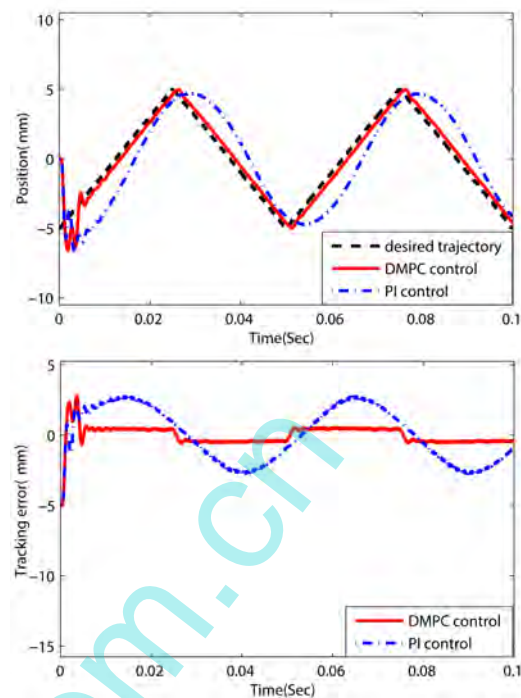Fig. 12. Tracking performance of both controllers for triangular waveform at 5Hz,10μm.

Fig. 13. Tracking performance of both controllers for triangular waveform at 20Hz,10μm.

controller, the proposed DMPC controller presents much better performance, mainly of much smaller tracking error.

B. Image Scanning for Samples

To further compare the proposed DMPC controller with the conventional PI controller, we implement both algorithms and employ them to scan certain samples in contact mode. Additionally, the feedback control law in z-axis is selected as PI controller with well tuned parameters to acquire the scanning images, by utilizing a MikroMasch CSC21/Cr-Au micro-cantilever made in Estonia.

Considering space limitation, we only present the scanning results for a calibration grating TCZ03 (μ Masch Inc. USA, nominal height: 500 nm, period: 3 μm) with the scanning range set as 10.5 $\mu m \times$10.5 μm. The images obtained from both methods under different frequencies of 5 Hz, 10 Hz and 50 Hz are shown in Fig. 16, with the left column for the proposed DMPC controller while the right one for the PI controller. As shown in Fig. 16 (a1), (b1), at comparatively low frequency of 5 Hz, both controllers yield accurate images for the detected sample. The quality of the images declines sharply as the scan frequency increases, especially for the conventional PI controller. In fact, when the scanning frequency is 50 Hz, PI controller can no longer provide trustworthy image, yet, the image obtained from the proposed DMPC controller still well describes the topography of the sample surface, mainly owning to the better tracking performance for triangular waveforms.

C. Applications

To further demonstrate the good performance of the proposed DMPC control algorithm, we have utilized the AFM

system to scan some typical samples. Due to space limitations, only the application results for a specimen of E. Coli bacillus are included in the paper as Fig. 17, with Fig. 17.(a) and Fig. 17.(b) depicting the images obtained at the scanning frequencies of 5 Hz and 20 Hz, respectively. It is clearly seen from Fig. 17 that the image constructed at 20 Hz is very close to the one obtained at 5 Hz, which sufficiently tells the superior performance of the designed DMPC tracking controller. It should be pointed out that the slight difference of the images in Fig. 17 is mainly caused by the thermal drift, which will be addressed in the future work.

Remark 3: In the experiments, the PT displacement is detected by the equipped capacitive sensor, whose measurement $v(V)$ is related to the PT displacement $x(\mu m)$ as follows:

$$x = \frac{10}{0.9521}v. \tag{25}$$

Remark 4: When testing the performance of the proposed DMPC controller, we have employed the PI controller for comparison since it prevails in currently available AFM systems. This practice is widely adopted when addressing AFM control problem [14], [32].

Remark 5: It can be seen from the results presented in Fig. 12 to Fig. 15 that, for different trajectories and distinct scanning frequencies, acceptable tracking performance is achieved for the developed AFM control system even with the same set of control gains, which shows good adaptability of the designed DMPC control algorithm. This is of much practical importance since it alleviates the burden of tuning control gains repetitively, and enables inexperienced operators to utilize an AFM without much difficulty.
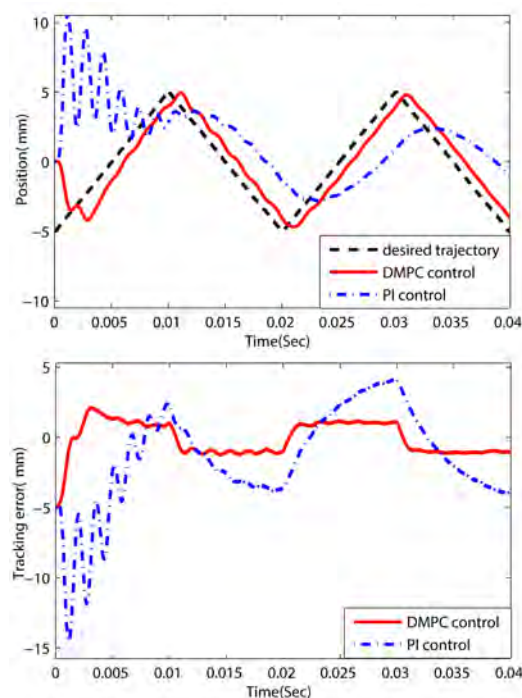
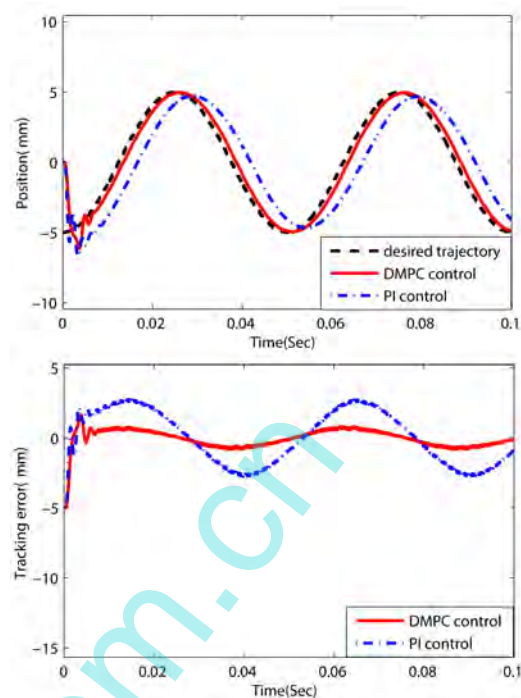Fig. 14.   Tracking performance of both controllers for triangular waveform at 50Hz,$10\mu m$.

Fig. 15.   Tracking performance of both controllers for sinusoidal waveform at 20Hz,$10\mu m$.

Remark 6: When the control gains for both the PI controller and the proposed DMPC algorithm are repeatedly tuned for different scanning frequencies, the experimental results can be further improved. Sufficient experiments show that under this situation, the DMPC algorithm achieves better performance than the conventional PI control law as well.

VI. CONCLUSIONS

For an AFM system equipped with a capacitive sensor, a varying-gain model is set up and experimentally verified, based on which, an advanced DMPC controller is designed to improve the tracking performance of the closed-loop system, so as to facilitate fast scanning tasks. Specifically, for an AFM system, the N4SID algorithm is firstly adopted to obtain a dynamic model, which is then combined with a gain adjustment mechanism to set up a varying-gain dynamic model with the measurement nonlinearity successfully considered. Based on the model, an advanced DMPC algorithm is designed, and then applied to a practical AFM system to accomplish exact tracking control for the desired triangular or sinusoidal trajectories. The proposed modeling/controller designing algorithm is utilized in a practical AFM system, and the collected experimental results show that the designed DMPC method provides much better performance than the conventional PI controller, and it is very promising to be employed for fast scanning tasks. In the future work, the proposed DMPC algorithm will be further put into effect for an AFM system to implement various high-speed scanning tasks. Besides, we will further study on how to propose more ambitious control/imaging algorithms to obtain satisfactory images when scanning at high speed.

REFERENCES

[1] C. A. Bippes and D. J. Muller, "High-resolution atomic force microscopy and spectroscopy of native membrane proteins", *Reports on Progress in Physics*, 74 (2011) 086601.

[2] M. Wu, W. Shih, Y. Tsai, Y. Chen, S. Chang, and P. Chang, "Rapid Dielectrophoresis Assembly of a Single Carbon Nanocoil on AFM Tip Apex", *IEEE Transactions on Nanotechnology*, Vol. 11, No. 2, pp. 328-335, Mar. 2012.

[3] J. Hou, L. Liu, Z. Wang, Z. Wang, N. Xi, Y. Wang, C. Wu, Z. Dong, and S. Yuan, "AFM-Based Robotic Nano-Hand for Stable Manipulation at Nanoscale", *IEEE Transactions on Automation Science and Engineering*, Vol. 10, No. 2, pp. 285-295, 2013.

[4] G. Binning, C. F. Quate, and C. H. Gerber, "Atomatic force microscope", *Phisical Review Letters*, Vol. 56, No. 9, pp. 930–933, 1986.

[5] G. Mangamma, S. Dash and A. K.Tyagi, "AFM investigations on N+ implanted TiN", *IEEE Transactions on Nanotechnology*, Vol. 12, No. 6, pp. 1007-1011, Nov. 2013.

[6] K. Igarashi, T. Uchihashi, A. Koivula, M. Wada, S. Kimura, T. Okamoto, M. Penttila, T. Ando, and M. Samejima, "Traffic jame reduce hydrolytic efficiency of cellulase on cellulose surface", *Science*, Vol. 333, pp. 1279-1282, 2011.

[7] Shiyou Ding, Yusan Liu, Yining Zeng, Michael E. Himmel, John O. Baker, and Edward A. Bayer, "How does plant cell wall nanoscale architecture correlate with enzymatic digestibility?", *Science*, Vol. 338, pp. 1055-1060, 2012.

[8] B. P. Brown, L. Picco, M. J. Miles and C. F. J. Faul, "Opportunities in High-Speed Atomic Force Microscopy", *Small*, Vol. 9, No. 19, pp. 3201-11, Oct. 2013.

[9] T. Ando, "High-speed atomic force microscopy coming of age", *Nanotechnology*, 23 (2012) 062001.

[10] C. Braunsmann and T. E. Schaffer, "High-speed atomic force microscopy for large scan sizes using small cantilevers", *Nanotechnology*, 21 (2010) 225705.

[11] Y. K. Yong, and S. O. R. Mohemani, "Design of an Inertially Counterbalanced Z-Nanopositioner for High-Speed Atomic Force Microscopy", *IEEE Transactions on Nanotechnology*, Vol. 12, No. 2, pp. 137-145, Mar. 2013.

[12] Y. Wei, C. Wu, Z. Dong, and Z. Liu, "Global Shape Reconstruction of the Bended AFM Cantilever", *IEEE Transactions on Nanotechnology*, Vol. 11, No. 4, pp. 713-719, Jul. 2012.

(a)   (b)

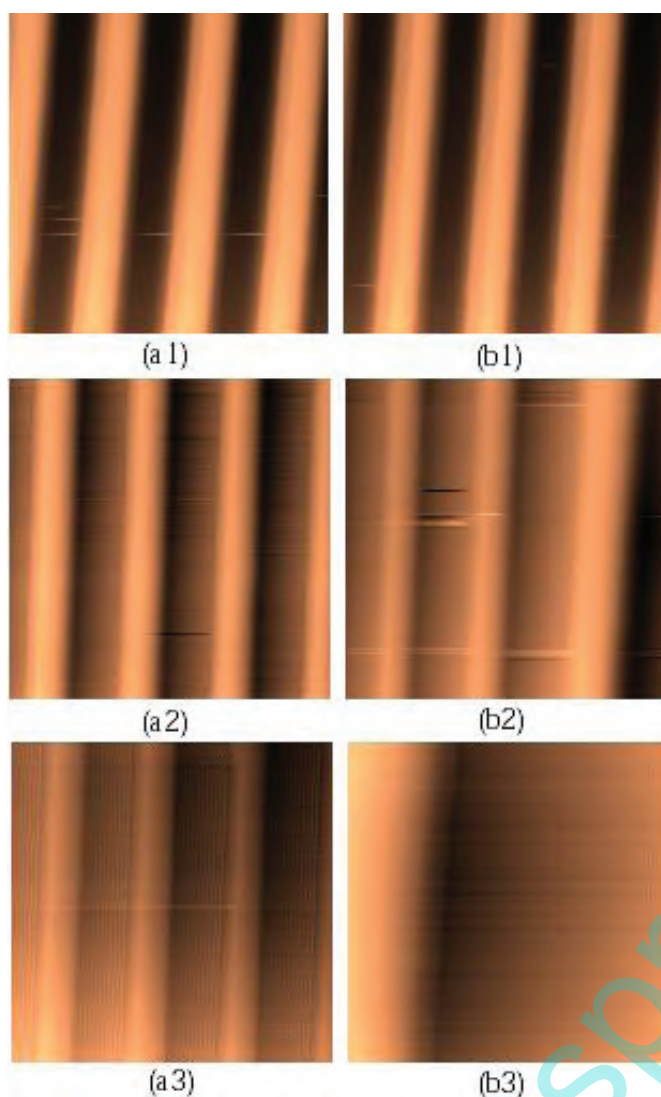Fig. 17. Scanned images of *E.Coli* bacillus specimen at 5Hz (a) and 20Hz (b).

Fig. 16. Images of calibration grating:(a1)-(a3) using the DMPC controller at 5 Hz, 10 Hz and 50 Hz, (b1)-(b3) using the PI controller at 5 Hz, 10 Hz and 50 Hz.

[13] Y. Qin, Y. Tian, D. Zhang, B. Shirinzadeh, and S. Fatikow, "A novel direct inverse modeling approach for hysteresis compensation of piezo-electric actuator in feedforward applications", *IEEE/ASME transactions on Mechatronics*, Vol. 18, No. 3, pp. 981-989, 2013.

[14] Habibullah, H. R. Pota, I. R. Petersen, and M. S. Rana, "Creep, Hysteresis, and Cross-coupling Reduction in the High-precision Positioning of the Piezoelectric Scanner Stage of an Atomic Force Microscope", *IEEE Transactions on Nanotechnology*, Vol. 12, No. 6, pp. 1125-1134, Nov. 2013.

[15] Yudong Zhang, Yongchun Fang, Xiaokun Dong, and Xianwei Zhou, "A novel learning control strategy for hysteresis and vibration of piezo-scanners", *Proc. of 48th Conference on Decision and Control*, 750-755, Shanghai, China, Dec. 2009.

[16] A. J. Fleming, and K. K. Leang, "Charge drives for scanning probe microscope positioning stages", *Ultramicroscopy*, Vol. 108, No. 12, pp. 1551–1557, 2008.

[17] Dong Wang, Zaili Dong, Niandong Jiao, Shuai Yuan, Lei Zhou, and Wen J. Li, "An asymmetric PI hysteresis model for piezoceramics in nanoscale AFM imaging", *Proceedings of the 2011 6th IEEE International Conference on Nano/Micro Engineered and Molecular Systems*, 1075–1079, Kaohsiung, Taiwan, Feb. 2011.

[18] Zhang Yudong, Fang Yongchun, Xianwei Zhou, and Xiaokun Dong, "Image-based hysteresis modeling and compensation for an AFM piezo-scanner", *Asian Journal of Control*, Vol. 11, No. 2, pp. 166-174, 2009.

[19] Babak Mokaberi, and Aristides A. G. Requicha, "Compensation of scanner creep and hysteresis for AFM nanomanipulation", *IEEE Transactions on automation science and engineering*, Vol. 5, No. 2, pp. 197–206, 2008.

[20] Guangyong Li, Yucai Wang, and Lianqing Liu, "Drift compensation in AFM-based nanomanipulation by strategic local scan", *IEEE Transactions on Automation Science and Engineering*, Vol. 9, No. 4, pp. 755–762, 2012.

[21] Ying Wu, and Qingze Zou, "Iterative control approach to compensate for both the hysteresis and the dynamics effects of piezo actuators", *IEEE Transactions on Control Systems Technology*, Vol. 15, No. 5, pp. 936–944, 2007.

[22] Kyong-Soo Kim, and Qingze Zou, "A model-free inversion-based iterative feedforward control for precision output tracking of linear time-invariant systems", *IEEE/ASME Transactions on Mechatronics*, Vol. 18, No. 6, pp. 1767-1777, Dec. 2013.

[23] Xiao Ren, Yongchun Fang, Ningning Qi, Ming Wu, Xizeng Feng, "A Practical Dynamic Imaging Method for Fast Scanning AFMs", *Instrumentation Science & Technology*, Vol. 41, Iss. 4, pp. 394-405, July 2013.

[24] C. Han, C. C. Chung, "Reconstruction of a scanned topographic image distorted by the creep effect of a Z scanner in atomic force microscopy", *Rev. Sci. Instrum.*, Vol. 82(5), pp. 053709, 2011.

[25] Qinmin Yang, S. Jagannathan, and E. W. Bohannan, "Automatic drift compensation using phase-correlation method for nanomanipulation", *IEEE Transaction on Nanotechnology*, Vol. 7, no.2, pp. 209-216, 2008.

[26] Ning. Chuang, Ian R. Petersen, and Himanshu R. Pota, "Robust H-infinity control in fast atomic force microscopy",*Proceedings of the 2011 American Control Conference*, 2258-2265, San Francisco, CA, USA, Jun. 2011.

[27] Y. Zhang, Y. Fang, J. Yu, and X. Dong, "Note: A novel atomic force microscope fast imaging approach: Variable-speed scanning", *Rev. Sci. Instrum.*, Vol. 82, pp. 056103-1C056103-3, 2011.

[28] Saeid Bashash, and Nader Jalili, "Robust adaptive control of coupled parallel piezo-flexural nanopositioning stages", *IEEE/ASME Transactions on Mechatronics*, Vol. 14, No. 1, pp. 11-20, 2009.

[29] Yongchun Fang, Yudong Zhang, Ningning Qi, and Xiaokun Dong, "AM-AFM Systems Analysis and Output Feedback Control Design with Sensor Saturation", *IEEE/ASME Transactions on Nanotechnology*, Vo. 12. No. 2, pp. 190-202, 2013.

[30] Wu Ying, Jian Shi, Chanmin Su, and Qingze Zou, "A control approach to cross-coupling compensation of piezotube scanners in tapping-mode atomic force microscope imaging", *Review of Scientific Instrument*, 80. 043709(1-10), 2009.

[31] Yuen Kuan Yong, Kexiu Liu, and S. O. Reza Moheimani, "Reducing cross-coupling in a compliant XY nanopositioner for fast and accurate raster scanning", *IEEE Transactions on Control Systems Technology*, Vol. 18, No. 5, pp. 1172-1179, 2010.

[32] M. S. Rana, H. R. Pota, and I. R. Petersen, "High-Speed AFM Image Scanning Using Observer-Based MPC-Notch Control", *IEEE Transactions on Nanotechnology*, Vol. 12, No. 2, pp. 246-254, Mar. 2013.

[33] Q. Xu and Y. Li, Model predictive discrete-time sliding mode control of a nanopositioning piezostage without modeling hysteresis, *IEEE Transactions on Control Systems Technology*, 2012, 20(4): 983-994.

[34] Peter Van O, and Bart DeM, "N4SID: Subspace algorithm for the identification of combined deterministic-stochastic system", *Automatic*, Vol. 30, No. 1, pp. 75–93, 1994.

[35] Iskandar A. Mahmood, S. O. Reza Moheimani, and Bharath Bhikkaji,

"A new scanning method for fast atomic force microscopy", *IEEE Transactions on Nanotechnology*, Vol. 10, No. 2, pp. 203–216, 2011.

[36] Yang Wang and Stephen Boyd, "Fast model predictive control using online optimization", *IEEE Transactions on Control Systems Technology*, Vol. 18, No. 2, pp. 267–278, 2010.
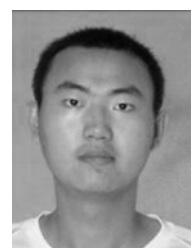
Ningning Qi received the B.S. degree in automation from Nankai University, Tianjin, China, in 2008. She is currently working toward the M.S. degree in the Institute of Robotics and Automatic Information System, Nankai University, Tianjin.

Her research interests include nanopositioning and adaptive control of atomic force microscopes.

Yongchun Fang (S'00−M'02−SM'08) received the B.S. degree in electrical engineering and the M.S. degree in control theory and applications from Zhejiang University, Hangzhou, China, in 1996 and 1999, respectively, and the Ph.D. degree in electrical engineering from Clemson University, Clemson, SC, in 2002.

From 2002 to 2003, he was a Postdoctoral Fellow with the Sibley School of Mechanical and Aerospace Engineering, Cornell University, Ithaca, NY. He is currently a Professor with the Institute of Robotics and Automatic Information System (IRAIS), Nankai University, Tianjin, China. His research interests include AFM-based Nano-systems, visual servoing, and control of underactuated systems including overhead cranes.

Xiao Ren received the B.S. degree in automation from Tianjin University, Tianjin, China, in 2011. He is currently working toward the Ph.D. degree in the Institute of Robotics and Automatic Information System, Nankai University, Tianjin.

His research interests include nanomanipulation, fast scanning atomic force microscopies, and nonlinear characters for piezo-scanners.
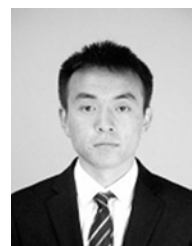
Yinan Wu received the B.S. degree in automation from Nankai University, Tianjin, China, in 2013. He is currently working toward the Ph.D. degree in the Institute of Robotics and Automatic Information System, Nankai University, Tianjin.

His research interests include compressive sensing ,nanomanipulation and nanopositioning of atomic force microscopes.